# Identification and Quantitation of Urea Precipitates in Flexible Polyurethane Foam Formulations by X-ray Spectromicroscopy

**E. G. Rightor,*,† S. G. Urquhart,‡,^ A. P. Hitchcock,§ H. Ade,‡ A. P. Smith,‡,|| G. E. Mitchell,† R. D. Priester,⊥ A. Aneja,# G. Appel,‡ G. Wilkes,# and W. E. Lidy⊥**

*Analytical Sciences, The Dow Chemical Company, 1897 Building, Midland, Michigan 48667; Department of Physics, North Carolina State University, Raleigh, North Carolina 27695; Brockhouse Institute for Materials Research, McMaster University, Hamilton, ON L8S 4M1 Canada; Polyurethanes, Dow Chemical, Building B-1608, 2301 N. Brazosport Blvd., Freeport, Texas 77541; and Department of Chemical Engineering, Virginia Polytechnic Institute and State University, Blacksburg, Virginia 24061*

*Received December 28, 2001*

ABSTRACT: Scanning transmission X-ray microscopy (STXM) and atomic force microscopy have been used to study the morphology and chemical composition of macrophase-segregated block copolymers in plaque formulations based on water-blown flexible polyurethane foams. Although there has been a large body of indirect evidence indicating that the observed macrophase-segregated features in water-rich polyurethane foams are due principally to urea components, this work provides the first direct, spatially resolved spectroscopic proof to support this hypothesis. The STXM results are consistent with a segregation model where urea segments segregate, forming enriched phases with the majority of the polyether−polyol and urethane groups at the chain ends of the urea hard segments. Chemical mapping of the urea, urethane, and polyether distribution about the urea-rich segregated phases showed that the urea concentration changes gradually (across several hundred nanometers) in a butylene oxide-based foam. This mapping also showed the urea-rich segregated phases present as a partial network in an ethylene oxide/propylene oxide sample.

## 1. Introduction

Phase segregation in water-blown elastomeric "flexible" polyurethane (PU) foams has been an issue of continuous debate and controversy since the first suggestion by Cooper and Tobolsky that diol-extended polyurethane elastomers possess a predominately two-phase morphology.[1] In water blown, flexible slabstock polyurethane (PU) foams this segregation is important since its appearance coincides with a substantial increase in viscosity, cell opening, and dimensional stability such that the foam does not suffer collapse.[2] It is also believed that details of the segregated structure are involved in providing the versatile and excellent properties of polyurethanes, leading to a wide range of applications.

A key feature of this segregation is the molecular structure of polyurethanes, which, though quite complex, can be considered as being comprised of alternating hard and soft segment units.[3] The soft segments are made of long chain polyethers or polyesters which are relatively flexible (subambient or low $T_g$) at ambient conditions. Reaction of hydroxyl moieties on the polyols with isocyanate moieties yields urethane linkages. The hard or rigid segments (glassy or high $T_g$) originate from reaction of isocyanate and a chain extender and have urea or urethane character. Additionally, water present in typical polyurethane foam formulations will undergo reaction with isocyanates to form carbamic acid, which decomposes to an amine and $CO_2$. Rapid reaction of the primary aromatic amine with additional isocyanate groups gives urea linkages which further builds the hard segment. For brevity, the term "urea", wherever used in this paper, will refer to these urea-based hard segments. The heat evolved due to the exothermic nature of the reactions along with the $CO_2$ produced helps to blow the foaming mixture and gives the foam its cellular structure. For reference, these basic reactions are illustrated in Scheme 1.

**Scheme 1**

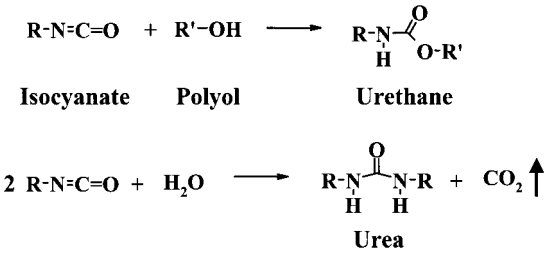


Because of the complexity of polyurethane reaction chemistry and morphology/structure development, the use of model systems has been vital to the development of the current understanding of polyurethane foams. Rossmy et al. showed using infrared spectroscopy of reactive and nonreactive polyethers that the urea hard segments initially formed stay in solution, but at a certain point they separate as a second phase due to their concentration and molecular weight buildup.[4] The occurrence of this microphase separation just precedes an increase in the viscosity of the foaming mixture and cell opening. The role of hard segment length on phase segregation is echoed in work by a number of different groups employing different analysis methods and chemi-

† Analytical Sciences, The Dow Chemical Company.
‡ North Carolina State University.
§ McMaster University.
⊥ Polyurethanes Research, Dow Chemical.
# Virginia Polytechnic Institute and State University.
^ Permanent address: Department of Chemistry, University of Saskatchewan, Saskatoon, S7N 5C9, Canada.
|| Present address: National Institute of Standards and Technology, Polymers Div., Gaithersburg, MD 20899.

10.1021/ma0122627 CCC: $22.00 
Published on Web 06/21/2002

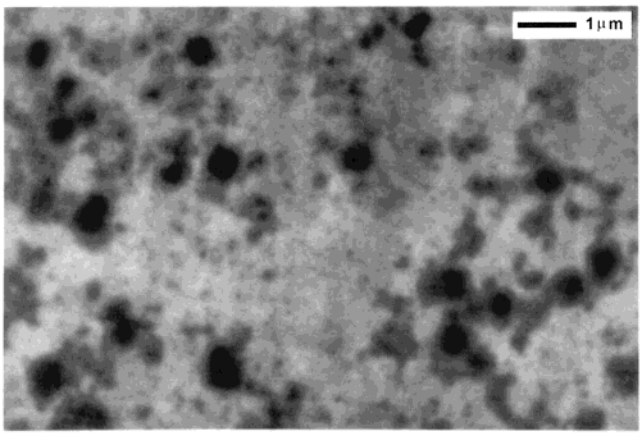


**Figure 1.** Transmission electron microscope (TEM) image of a high water slabstock polyurethane made from poly(butylene oxide) (BO)-based polyol. This is the same BO-based sample that was studied by STXM.

cal models.[5−7] In situ studies by infrared spectroscopy[8−13] and X-ray scattering[10−13] have reinforced these ideas and added information on the phase separation kinetics and subsequent structure/morphology development.

Armisted et al. found that when the water content is increased, a bimodal distribution of hard segments occurs where one component of the distribution consists of small hard segment microphase-separated domains and the other component is hard segment rich aggregates which are 100−300 nm in size.[7] Historically, these hard segment aggregates have often been called urea "balls" or urea "precipitates",[3] although the molecular structure being dominated by urea was, until the present work, only inferred, not based on microanalytical results. We use the term *macrophase* to distinguish them from the very small hard segment domains (<5 nm) or microsegregated phases which are detected commonly by small-angle X-ray scattering (SAXS). For foams made with a water content of 3 pph (parts per hundred parts polyol) or greater the macrophases are evident in transmission electron microscopy (TEM) (even without heavy element staining) as dark, diffuse clusters (see Figure 1). Dynamic mechanical spectroscopy (DMS) showed that increasing the water level (and hence hard segment content) resulted in increased modulus. However, the location of the soft segment glass transition temperature ($T_g$) was not affected, indicating that there is little additional incorporation of urea into the soft, polyol-rich phase with increasing water content. Wide-angle X-ray scattering (WAXS) showed relatively sharp peaks which sharpen with increasing hard segment content. The latter effect was interpreted in terms of increasing order in the hard segments. Small angle (SAXS) showed that the relative size of the microphase-segregated hard phase did not change with water content.

Studies of the influence of polyol structure and chain extenders on macrophases have shown that the addition of relatively low levels of diethanolamine (DEOA) eliminates the macrophases.[14] Their presence can also be altered and eliminated by addition of small amounts of LiCl.[2] Macrophase precipitates are common in slabstock foams but are absent for high-resiliency (HR) polyurethane foams where DEOA or other cross-linkers are used, polyols of high molecular weight are ethylene oxide (EO) capped giving a high primary OH content, and low-potency surfactants are employed.[14−18] HR polyols typically exhibit improved compatibility with the toluene diisocyanate (TDI) used and water. This absence of macrophase precipitates for HR materials agrees with the dependence of macrophase segregation on water solubility in the polyol/TDI blend.[17] DEOA competes with water and polyol OH groups for the isocyanate which influences the polymer morphology development and phase segregation.[18] While HR foams have many desirable properties, they generally have lower tensile strengths, tear resistance, elongation properties, and air flow than slabstock foams. The contribution of the macrophases to these favorable properties and their role in cell opening is of continuing interest to help understand how to further optimize polyurethane formulations for specific applications.

In optimizing polyurethane foams, an important question is whether modification of the morphology and amount of these macrophases can directly or indirectly influence physical properties. Hence, the way that they interconnect with the matrix and potentially with one another (e.g., network) is important. The chemical nature of these macrophase precipitates, and their purity is also central to determining their influence on properties. Since additional water reacts with TDI to make urea linkages, it has been assumed that the macrophases are composed of polyurea-based hard segments. Elwell et al. state, for a range of water contents studied, that the microphase separation transition (MST), where free urea decreases and bidentate urea rapidly is formed, in methylene diphenyl diisocyanate (MDI)-based systems takes place at an isocyanate conversion of 0.55 (i.e., 55% of initial MDI has reacted).[19−21] Once the urea segment length exceeds a critical value in the reacting polymer mixture macrophase segregation can occur. While this explanation of urea precipitation is likely, there are other possible hypotheses, given the myriad of side reactions known to be possible in polyurethane chemistry. It is also possible that isocyanureate or trimers (a cyclic urea formed from the reaction of three isocyanate groups) could play a role in formation of macrophase precipitates. There are other possibilities such as biuret (a double urea) or allophanate (a urethane−urea combination) that, while less likely, have not been conclusively eliminated as possibilities for the macrophases.

Although infrared spectroscopy has the spectral sensitivity to distinguish the different species formed in polyurethanes, spectral overlaps in the carbonyl region greatly complicate analyses. The use of deuterium oxide can minimize these overlaps,[22] but to our knowledge this method has not been used specifically to address the issue of macrophases. In addition, the state-of-the-art spatial resolution of current infrared (∼5 $\mu$m) and Raman (∼0.5 $\mu$m) microscopy does not allow direct study of the macrophases. Transmission electron microscopy and associated spectroscopic methods such as electron energy loss spectroscopy (TEM-EELS) have the necessary spatial resolution. These have been explored by us and others to characterize the macrophases spectroscopically, but high radiation damage rates and insufficient chemical specificity due to limited energy resolution have thwarted productive studies.

The recent development and application of X-ray spectromicroscopic methods[24−28] have opened new paths for directly determining the chemical identity of the macrophases. These methods can deliver spatial resolution better than 50 nm,[27,29] have much lower radiation

damage than TEM,[28] and have very high spectral resolution (~0.1 eV in the C 1s region). All of these capabilities are crucial to directly exploring the complex chemistry and morphology of polyurethanes at a spatial scale below 0.5 $\mu$m. To fully utilize the spectra obtained, quantitative reference spectra have been measured, and key transitions relating to chemical functional groups have been identified in both TDI- and MDI-based polyurethanes using a combination of core edge spectroscopy of gas-phase analogues, X-ray spectroscopy of model polymers, and molecular orbital theory calculations.[29−31]

Atomic force microscopy (AFM) is now a well-established technique to study polymer morphology. McLean and Sauer have demonstrated the use of AFM to obtain nanophase information at the hard domain level of a segmented polyurethane system.[32,33] Kaushiva et al. recently utilized AFM to study slabstock polyurethane foam materials.[34] The use of AFM to study plaques based on molded polyurethane foams has also been reported by others.[35,36] All of these studies have used AFM in tapping mode which reduces the contact time between the tip and the sample and also involves considerably lower forces as compared to contact mode AFM.

In the present work we have used scanning transmission X-ray microscopy (STXM) to obtain direct chemical information on these macrophases in order to elucidate their nature and map the distribution of chemical components. Two plaques based on flexible polyurethane foam formulations were chosen for study: one made with an all-butylene oxide (BO)-based polyol and the other, a more conventional polyol, made with ethylene oxide and propylene oxide (EO/PO) repeat units. While EO/PO polyols are typical for flexible polyurethanes, BO polyols have been used[37] in flexible as well as in rigid foams[38] where their presence serves as a compatibilizer, allowing higher concentrations of nonhalogenated hydrocarbon blowing agents and thus maintaining relatively lower water content. Macrophase precipitates have been observed in all high water BO-based and EO/PO formulations as well as in all high water PO-based foams studied earlier.[7] The X-ray microscopy of the EO/PO formulation has been complemented with AFM studies.

## 2. Experimental Section

The formulations for the TDI-based polyurethane plaques used for this study are summarized in Table 1. The all-BO polyol sample was made as a plaque using procedures reported previously.[3] The as-made material was milky white in appearance, suggesting the structures present were on the size scale of the wavelength of light. The preparation of the EO/PO plaque was carried out in a lab scale cup-foaming setup at The Dow Chemical Co. in Freeport, TX. Preweighed amounts of water and polyol were added in a 400 mL beaker and stirred for 25 s at 2000 rpm with a 1 in. diameter stirrer. The TDI and the catalyst were then added, and the mixture was stirred for another 15 s at the same stirring speed. Stirring was then continued by hand using a tongue depressor to prevent the formation of a stable cellular structure. Just prior to gelation, the reacting mixture was quickly poured onto Teflon sheets supported by steel plates and placed in a hot press operating at 100 °C and 98 000 kg/m$^2$ for 1 h. A picture-frame mold with dimensions of ca. 6.5 × 6.5 × 0.05 in. was utilized. At the end of 1 h, the plaque was cut out from the picture-frame mold and allowed to cool at ambient conditions.

X-ray spectromicroscopy was carried out using the Stony Brook STXM at beamline X1A at the National Synchrotron Light Source (NSLS, Brookhaven, NY)[23,24,39] and the Advanced Light Source (ALS, Berkeley, CA) beamline 7.0 STXM.[40,41] The energy resolution was typically 0.1 eV fwhm (full width half-maximum). Thin sections of the sample were prepared using a Reichert-Jung (now Leica) microtome with cryo-attachment at −120 °C. Samples were transferred dry to unsupported copper grids with an eyelash. Energy scales were calibrated by adding $CO_2$ gas to the He purge in the microscope and recording the transmission spectrum of the mixture of the polymer and $CO_2$ gas.[39] The energies of the $CO_2 \rightarrow$ Rydberg transitions from the high-resolution near-edge X-ray absorption spectra (NEXAFS) of Ma et al.[42] were used to calibrate these spectra.

**Table 1. Formulations for the Two High Water Polyurethanes Investigated**

| component | amount (parts per hundred parts of polyol) (w/w) | |
|---|---|---|
| | BO-based foam | PO/EO-based foam |
| polyol | 100 (exptl)[a] | 100 VORANOL 3137[b] |
| TDI[c] | 65.47 | 52.0 |
| water | 6 | 4.5 |
| catalyst (DABCO* 8263)[d] | 0.12 | |
| catalyst T9[e] | 0.12 | |
| catalyst DABCO*[f] 33LV/ DABCO* BL11 5/1 w/w | | 0.2 |
| surfactant | none | none |

[a] The butylene oxide (BO) polyol was a 3000 MW glycerine initated, all BO triol (Dow) with a BO 3000 MW triol (15170 triol). [b] VORANOL 3137 is a glycerol initiated PO/EO random adduct. [c] TDI is toluene diisocyanate (Dow, with a 2,4 to 2,6 isomer ratio of 80). [d] DABCO$^+$ 8263 is an amine catalyst blend optimized for slabstock foams. [e] T9 is stabilized stannous octoate. [f] DABCO$^+$ 33LV and BL11 are amine catalysts from Air Products.

The NEXAFS spectra used to determine the chemical composition in various regions of the sample were obtained either (i) using a stationary focused point probe or (ii) by postacquisition data processing of an image sequence (also called a "stack" sequence).[43] Analysis involved quantitative least-squares fitting to a linear combination of reference spectra. (The sources of materials used for reference spectra are indicated in the tables.) The point spectra of matrix and precipitates that are presented here were acquired with a fully focused X-ray beam with a 50 nm spot size. Careful tuning of the Stony Brook STXM was essential in order to reduce the pointing error to below 50 nm over the full energy range of the NEXAFS spectra. The image sequence alignment of data sets acquired at both the Stony Brook and BL7.0 STXMs was done using a combination of manual alignment on fiducial points of the image and by Fourier transform-based cross-correlation methods.[43] There is some residual jitter in the aligned images, but it is quite small (<50 nm, similar to the spatial resolution) and does not detract from the precipitate analysis. The larger precipitates used for quantitative analysis were 12−14 pixels across (700 nm).

Atomic force microscopy experiments were performed in the tapping mode to observe the presence of the micron size urea aggregates. A Digital Instruments scanning probe microscope employing a Nanoscope IIIa controller and Nanosensors TESP (tapping etched silicon probe) type single-beam cantilevers were utilized to carry out the scans. The cantilevers had nominal lengths of 125 $\mu$m, with force constants in the range of 35 ± 7 N/m, and were used at oscillation frequencies of ca. 295 kHz. The tips had nominal radii of ca. 5−10 nm. Small pieces of the sample were cut out from the plaque and embedded in epoxy which was allowed to cure overnight at ambient conditions. The sample dimensions were found to be unchanged after the surrounding epoxy had cured; i.e., no swelling occurred. A razor blade was used to expose a small cross section of the sample by trimming away the surrounding epoxy. The exposed cross section was cryogenically microtomed using a Reichert-Jung Ultracut E ultramicrotome equipped with a model FC-4D cryo-attachment operating at −90 °C. The cryotomed surface was then examined via AFM.

The AFM images presented in this paper are representative of the bulk morphology of the material. Both "height" and "phase" images were collected, but the height images showed little contrast, consistent with a smooth microtomed surface and a uniform section thickness, as deduced from the quantitative STXM analysis (see below). In phase images obtained by *t*-AFM, a higher modulus material typically induces a higher phase offset and appears lighter as opposed to a softer phase which appears darker. Thus, for the materials imaged in this investigation, the urea-rich regions appear lighter where as darker regions correspond to the softer polyol phase. The free air oscillation amplitude was set at 60 nm, and the amplitude of the tip while striking the surface was maintained at ca. 66% of this value.

Transmission electron microscopy (TEM) was similar to that reported previously.[18]

## 3. Results and Discussion

**3.1. STXM of High Water Polyurethanes: Basis for Chemical Identification.** Figure 1 is a typical TEM image illustrating the morphology of the macrophase precipitates observed in the BO-based high water slabstock plaque. The fact that these precipitates are observed with fairly high contrast in unstained sections suggests either a chemical (elemental) or a density variation between the matrix and the precipitates. Paracrystalline ordering was implicated in an earlier study based on increasing sharpness of WAXS peaks with increasing water content,[7] but it is unclear whether this level of ordering contributes to the contrast observed by TEM. It is unlikely that section thickness varies on the size scale of the precipitates due to the cryomicrotomy. This contrast was shown to be mainly chemical in origin by the multiple energy X-ray microscopy described below. Comparisons of X-ray images recorded at different energies provides a powerful means of distinguishing chemical from density/thickness contrast.

To apply NEXAFS microscopy to mapping of chemical species in our polyurethane materials, characteristic transitions of the species of interest—mainly the TDI−urea, TDI−urethane, and EO/PO and BO polyols—have been identified by studying the spectroscopy of molecular analogues and model polyurethane polymers.[29−31] From this body of work, the C 1s NEXAFS spectra for the main components of a TDI-based polyurethane are presented in Figure 2. The spectra show several transitions of interest for measuring the chemical composition of polyurethanes. The strong peak at 285.2 eV arises from C 1s(C−H) → $1\pi^*_{C=C}$ transitions at the C−H carbons of the phenyl rings. The presence of this peak is a clear indicator of aromatic groups (ureas or urethanes) from the reaction with TDI and distinguishes these components from the aliphatic polyol. The peak at 286.6 eV is the C−R peak due to carbons attached to pendant groups. At 289.5 eV there is a strong, sharp feature for the urea associated with C 1s(C═O) → $\pi^*_{C=O}$ transitions. The corresponding C 1s(C═O) → $\pi^*_{C=O}$ feature in the urethane structure occurs 0.5 eV to higher energy, at 290.0 eV. This energy difference is well within the spectral resolution at the two STXM microscopes (in each case, near 0.1 eV) and provides a key handle for differentiating and mapping the urea and urethane groups in the polymer.

The strongest feature in the C 1s spectrum of the BO or EO/PO polyol component is a relatively broad structure peaking at 289 eV which is associated with overlapping C 1s → $\sigma^*_{C-H}/\sigma^*_{C-C}$ transitions in the polyether chains. This peak occurs just before the carbonyl transitions of the TDI−urethane and TDI−urea which complicates distinction of the carbonyl signal relative to the polyol background, given that the polyol concentration of a typical slabstock polyurethane is nearly 70 wt %. Thus, while the main functional groups do have distinguishable spectral features, procedures to deal with spectral overlap are needed. The energies of the characteristic features and assignments for all the transitions[31] are summarized in Table 2.

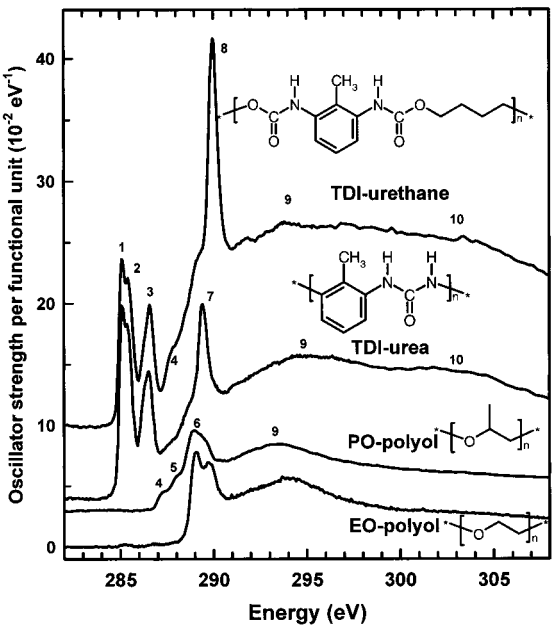


**Figure 2.** NEXAFS spectra[31] of 2,6-TDI−urethane, 2,6-TDI−urea, poly(propylene oxide) (PO), and poly(ethylene oxide) (EO), the main components of one of the two TDI-based polyurethanes examined. The PO spectrum was extracted from a high molecular weight polyol polyurethane (TDI−V2100) and has had a small amount of TDI−urethane subtracted to remove the microphase hard segment contribution from that sample. The other three spectra are as-recorded from reference polymers. Energies and assignments of the numbered features are indicated in Table 2.

Figure 3 presents C 1s spectra of the precipitates and matrix of the BO polyol-based plaque sample as well as optical density images at four selected energies, and the ratios of the images at 285.2, 287.5, and 289.7 eV to that at 332 eV, to eliminate the effect of thickness/density variations. The macrophase precipitates are seen at all energies but most clearly at 285.2 eV. Their size and appearance are similar to those seen in TEM (Figure 1 and ref 7). By tuning the energy of the incident radiation in the 285−292 eV region to coincide with spectral peaks associated with individual chemical components, the image contrast changes significantly, as shown in this figure. This shows that STXM is sensitive to the presence of key functional groups even with the high amount of polyol present in a typical slabstock polyurethane. These contrast changes can be used to determine the spatial distribution of these groups. To differentiate chemical and density/thickness contrast, each image has been converted to optical density scale and normalized to the aligned optical density image at 332 eV, which is proportional to the carbon atom density. The persistence of the macrophase features in the ratio image indicates that chemical contrast is much larger than density differences. In the following, detailed analysis of point spectra are used to

**Table 2. Energies and Assignments of Characteristic C 1s Spectral Features of Polyurethane Components (from Ref 31)**

| peak no. | polyol[a] | | TDI−urethane[b] | | TDI−urea[b] | |
|---|---|---|---|---|---|---|
| | *E* (eV) | assignment | *E* (eV) | assignment | *E* (eV) | assignment |
| 1 | | | 285.16[c] | $\pi^*_{C=C}$ (C−H) | 285.16[c] | $\pi^*_{C=C}$ (C−H) |
| 2 | | | 285.44 | $\pi^*_{C=C}$ (C−H) | 285.44 | $\pi^*_{C=C}$ (C−H) |
| 3 | | | 286.65 | $\pi^*_{C=C}$ (C−R) | 286.55 | $\pi^*_{C=C}$ (C−R) |
| 4 | 287.4 | Ryd/$\sigma^*_{C-H}$ | 287.5 | $\sigma^*_{C-H}$ | 287.8 | $\sigma^*_{C-H}$ |
| 5 | 288.1 | Ryd/$\sigma^*_{C-H}$ | | | | |
| 6 | 289.1[c] | $\sigma^*_{C-O}$ | | | | |
| 7 | | | | | 289.5 | $\pi^*_{C=O}$ |
| 8 | | | 289.9 | $\pi^*_{C=O}$ | | |
| 9 | 294 | $\sigma^*_{C-C}$ | 294 | $\sigma^*_{C-C}$ | 294 | $\sigma^*_{C-C}$ |
| 10 | | | 304 | $\sigma^*_{C=C}$ | 302 | $\sigma^*_{C=C}$ |

[a] These values refer to the peaks in the PO−polyol spectrum. Similar peaks are found in EO− and BO−polyol. The PO−polyol spectrum plotted in Figure 2 is taken from the spectrum of a high molecular weight polyol polyurethane (TDI−V2100) and has had a small amount of TDI−urethane subtracted.[31] The spectrum of EO−polyol was that of a 5 MDa commercial sample.[31] [b] The TDI−urethane and TDI−urea (80:20 mix of 2,4 and 2,6 isomers) were synthesized for the model compound study.[31] [c] Calibration via gaseous $CO_2$.[31]

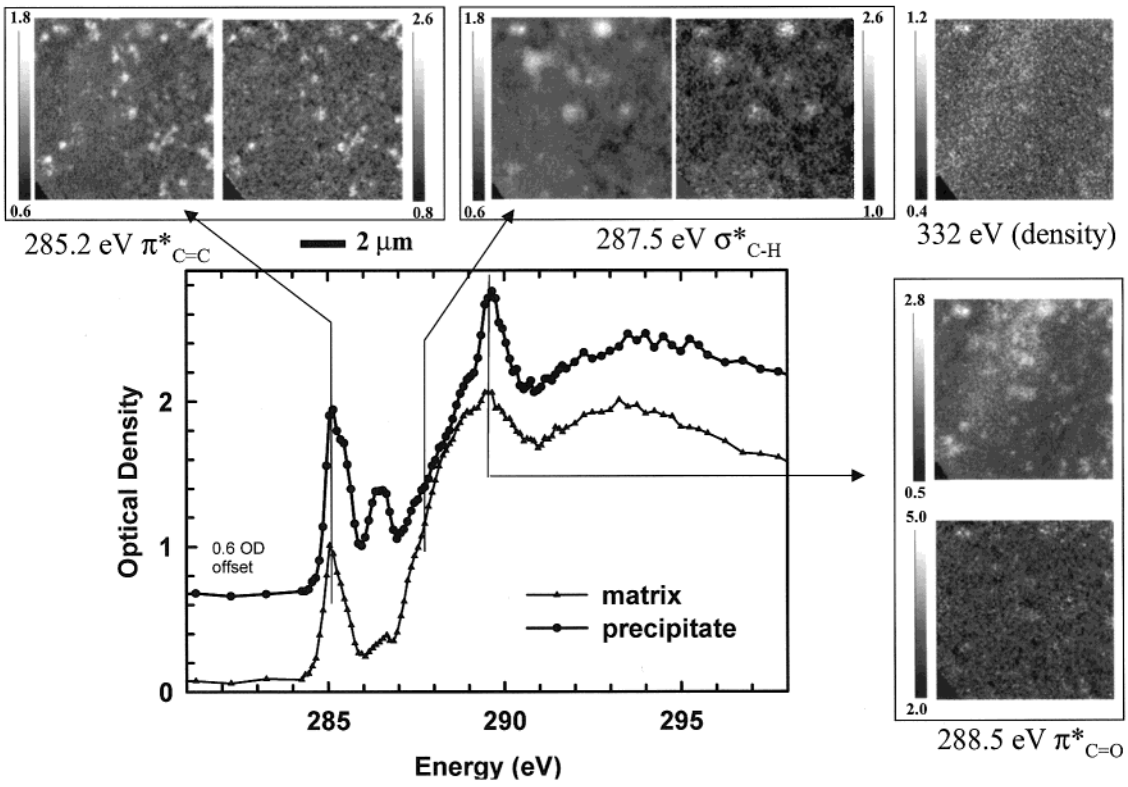


**Figure 3.** Optical density (OD) images at four energies (285.2 eV, phenyl ring $\pi^*_{C=C}$; 287.5 eV, $\sigma^*_{C-H}$ of polyol; 289.5 eV, $\pi^*_{C=O}$ of urea; and 332 eV, carbon density) and selected area spectra of a high water, BO-based, slabstock polyurethane. These images are part of an image sequence of the BO-based polyurethane. The small, dark triangle at the lower left in each image is the edge of the section (i.e., a hole). The signal in this region was used for incident flux normalization. In each image pair the one to the left (or for 289.5 eV the top one) is the optical density (OD) image while the one labeled "ratio" is the ratio of that image to the OD image at 332 eV, to remove density contrast effects. The similarity of the contrast in the ratio and OD images, particularly at 285.2 eV, indicates most of the contrast arises from chemistry rather than density or thickness variations. A small systematic noise pattern was removed from the 332 eV image by 2-d Fourier filtering.

determine composition of the matrix and macrophase precipitates, while sets of energy specific images are used to quantitatively map the distribution of the urea, urethane, and polyol moieties.

**3.2. Quantitative Composition and Morphology of Macrophase Precipitates in BO-Based Plaques.** Figure 4 shows results of a study of the composition of macrophase precipitates vs matrix using C 1s spectra acquired in the "point" spectral mode at the regions indicated by the arrows. The spectra of four areas of the "matrix" and four macrophase precipitates were measured, and these spectra were averaged to improve the statistical precision of the signal. The quantitative amounts of urea, urethane, and polyol in the precipitates and in the matrix are summarized in Table 3. These values were determined using a least-squares fit of the experimental data to spectral models from TDI polymers (Figure 2[31]). The model spectra were placed on intensity scales reflecting the optical density of a 1 nm thick sample of the pure material, and thus the weighting coefficients from the fit give the equivalent thickness of the sample. The aromatic peaks (285.2, 286.5 eV), which can be due only to either the urea or urethane, were key to this process. Additionally, the fit to the carbonyl peak near 289 eV was important as its shape and position reflect the relative amounts of urea and urethane in the sampled region of the polymer.

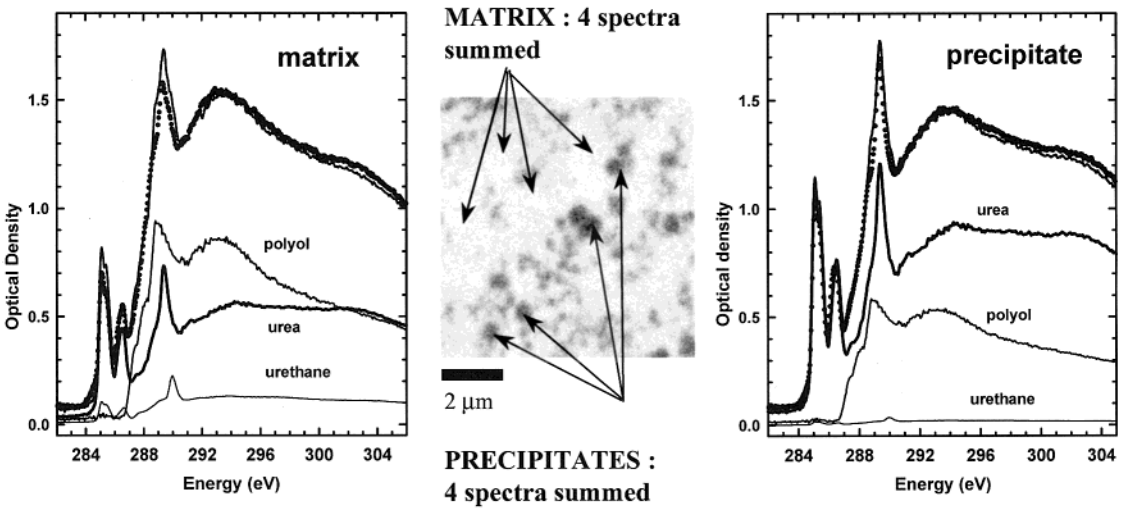


**Figure 4.** Transmission image at 285.2 eV of the BO-based polyurethane. Point spectra were acquired with a fully focused beam (~50 nm) at the ends of the arrows. The average of four matrix spectra is plotted as the data points in the left-hand plot which also includes a fit to a linear combination of the standard components. A similar presentation is made for the average of the four precipitate spectra in the right-hand plot. The compositions deduced from the fitting are summarized in Table 3.

**Table 3. Quantitative Analysis[a] of Composition of Matrix and Precipitates of Two High Water Polyurethanes**

| | polyol | | urethane | | urea | |
|---|---|---|---|---|---|---|
| sample | $t^b$ (nm) | vol %[c] | $t$ (nm) | vol % | $t$ (nm) | vol % |
| (a) Matrix | | | | | | |
| (BO)−point | 104 | 47 | 20 | 9 | 99 | 44 |
| (BO)−image sequence | 157 | 58 | 31 | 12 | 81 | 30 |
| (EO/PO)−SVD | 307 | 77 | 28 | 7 | 65 | 16 |
| (b) Precipitate | | | | | | |
| (BO)−point | 64 | 28 | 5 | 2 | 163 | 70 |
| (BO)−image sequence | 58 | 19 | 48 | 16 | 201 | 65 |
| (EO/PO)−SVD | 230 | 43 | 60 | 11 | 246 | 46 |

[a] The C 1s spectrum of the matrix or macrophase precipitate on the as-recorded optical density scale was fit to model spectra which had been converted to optical density for 1 nm thickness by normalizing outside the structured region to an optical density per nm computed from the X-ray transmission of the same elemental composition (see Figure 2 for formula unit structures).[51] The assumed densities were 1.106 g/cm$^3$ for polyol and 1.251 g/cm$^3$ for urethane and urea.[49] Astack fit was used for the many image sequence (BO) and SVD for the few image sequence used in studying the EO/PO sample. [b] $t$ is the thickness in nm deduced from the weighting coefficient of the fit. [c] Vol % is the percentage of the total thickness in the region sampled.

Figure 5 shows details of a corresponding quantitative analysis of spectra recorded in the image sequence mode for the BO-based polyurethane. We averaged the spectra using pixels from several precipitates and several matrix regions in order to improve the statistical precision of the average matrix and average precipitate spectrum. The quantitation results from the two methods are compared in Table 3. Overall, there is good agreement with the quantitation found for the EO/PO polyurethane (see next section). However, the fits of the matrix demonstrates that there are slight differences between the chemistry expected on the basis of the polymer models and that found in the matrix. The aromatic peak due to the urea (very little urethane present) in the data is greater than the fit while intensity of the C−R peak however is lower. Spectra from the point mode during a different data collection at the same microscope show a stronger C−R peak as expected. It is possible that some radiation damage had occurred, although images taken after the image stack showed no mass loss. If present, damage should reduce

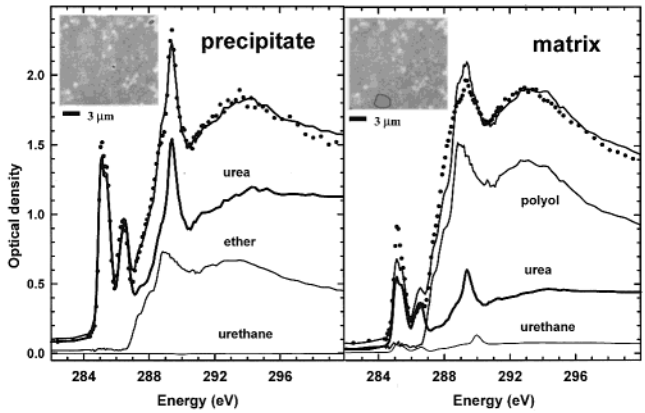


**Figure 5.** Examples of fits to spectra of the precipitate and matrix regions of a BO-based high water polyurethane extracted from an image sequence. The spectra (points) were obtained by summing the signals in the areas indicated in the accompanying 285.2 eV OD image. The compositions deduced from the fitting are summarized in Table 3.

the intensity of the carbonyl while the C−R and $\pi^*$ ring (at ~285 eV) should be largely unaffected.[44] The differences could also be due to the presence of additional components which are not accounted for using the three polymer model components, although they worked very well for the point spectra in Figure 4 and for the precipitate spectrum from the image sequence. As mentioned above, there are numerous reactions possible in polyurethane chemistry other than those shown in Scheme 1. A more precise spectral analysis requires further research.

These STXM results show that the main component of the macrophase precipitates is indeed TDI−urea and that the ratio of urea to urethane increases by about a factor of 3 from the matrix to the precipitates. The amount of urethane in the precipitates is very small, and the amount of polyol is also lower than in the matrix. Although there has been a large body of indirect evidence indicating that macrophase-segregated features in water-rich polyurethanes are urea dominated, this is the first direct, spatially resolved proof that these macrophase regions are dominated by TDI−urea. The STXM results are consistent with a segregation model[4,7] where ureas segregate forming enriched macrophases,

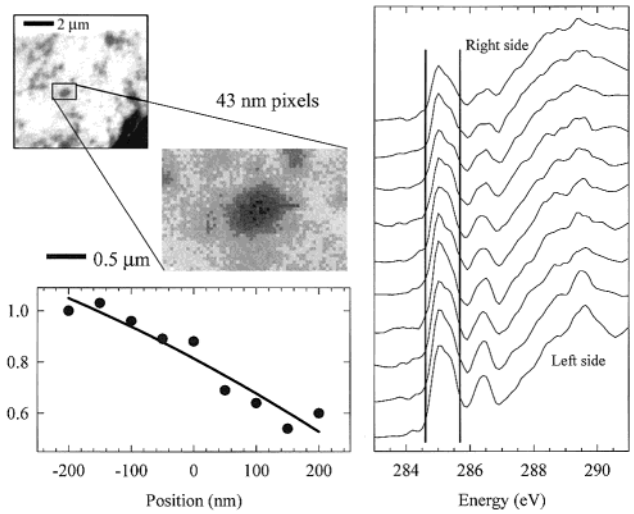


**Figure 6.** Spectra at pixels along a line over the boundary of a precipitate and the adjacent matrix indicated in the associated transmission image. The changes in the spectra indicate there is a continuous variation of urea from the core of the precipitate relatively far into the adjacent matrix. The lower right plot indicates the integrated intensity of the 285.2 eV peak across the boundary or interface between the precipitate and the matrix. The spatial resolution was about 50 nm.

and the majority of polyol and urethane is present at chain ends of the polyureas.

Another look at the spectra in Figure 4 shows that, since the precipitate spectra are dominated by the contribution from urea in the spectral region due to aromatic transitions, the intensity of the 285.2 eV peak in the macrophase precipitates is a reasonable way to map the amount of urea in the precipitates. In the matrix, the 285 eV intensity comes primarily from a low level of urea, although there is a weak contribution from urethane. For the matrix the 285.2 eV image should be primarily related to the urea distribution, but there will be a small contribution from the urethane.

Figure 6 shows spectra from pixels along a line across a precipitate−matrix boundary (extracted from an image sequence) in order to examine the chemical variation of urea present in a precipitate. A plot of the intensity at 285.2 eV across the boundary or interface between the precipitate and the matrix is also shown in Figure 6. The spectral transition across the precipitate−matrix boundary is very broad, indicating that the precipitates are relatively diffuse. This analysis also shows that the urea concentration continues to decline a substantial distance past the region of high contrast in an image. The diffuse nature of the precipitates contrasts with the sharp delineation of the "urea balls" as envisioned prior to this study.[3]

**3.3. Quantitative Composition and Morphology of Macrophase Precipitates in EO/PO Plaques.** Figure 7 (upper left) shows the optical density image at 285.2 eV of the EO/PO-based plaque. Singular value decomposition (SVD)[45−48] was used to determine the spatial distributions of the three major components, EO/PO−polyol, TDI−urea, and TDI−urethane, from STXM images. Figure 8 presents examples of fits to selected matrix and precipitate regions, with results summarized in Table 3. Analysis of the EO/PO plaque shows that the urea content of the precipitates is about 3 times higher than that of the matrix. This is similar to the results for the BO-based plaque sample. It is difficult to determine the concentration of urethane in the matrix

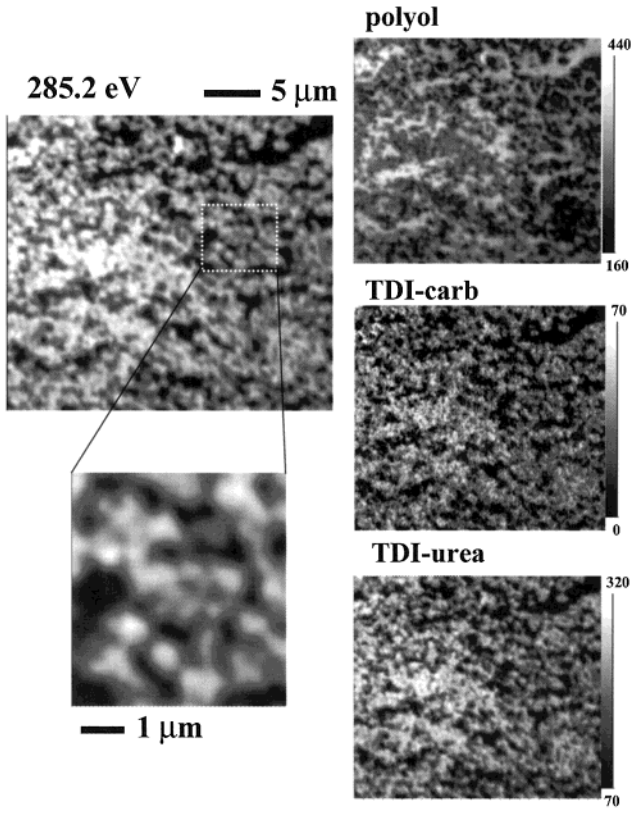


**Figure 7.** (left) Optical density image at 285.2 eV of a high water EO/PO-based polyurethane. The expanded presentation (lower left) strongly suggests that the urea-rich precipitates are linked forming a hard segment network. (right) Component maps derived by singular value decomposition of a 19 image sequence. The vertical scales are thickness in nanometers.

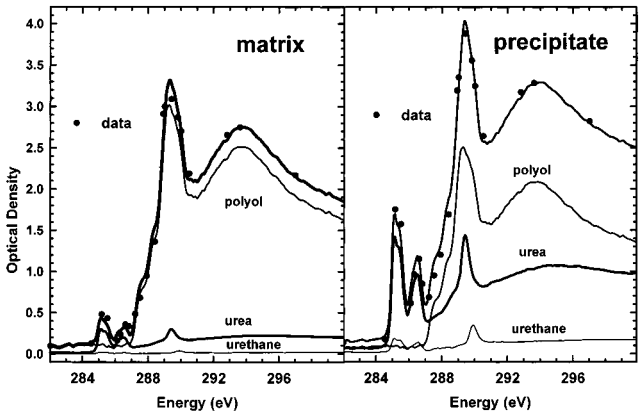


**Figure 8.** Fits to matrix and precipitate spectra extracted from the image sequence recorded from the high water EO/PO-based polyurethane (Figure 7). The compositions deduced from the fitting are summarized in Table 3.

accurately since the amount is very low. The analysis suggests small amounts of urethane may be present in the macrophases with even less urethane in the matrix. Also, the results suggest that there is some polyol in the macrophases, albeit much less than in the matrix. Although these images are two-dimensional projections of a three-dimensional structure, the sample sections studied by STXM (∼200 nm) are thinner than the size of the precipitates (200−500 nm) so it is unlikely that the polyol detected at the spatial location of the precipitates is actually above or below the precipitates. Additional evidence for polyol segregated in the precipitates is given in the AFM images below.

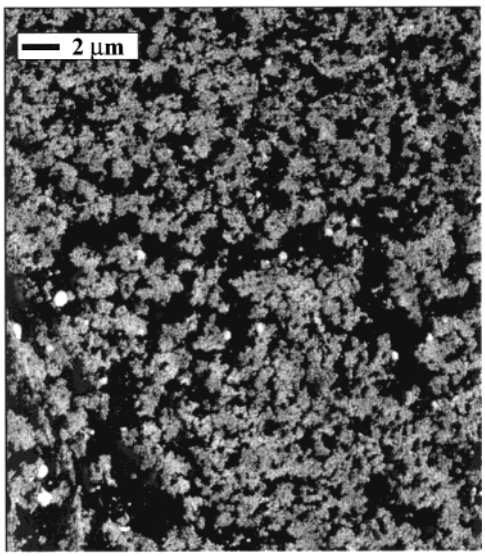


**Figure 9.** AFM phase image ($25 \times 25\ \mu m^2$) of the high water EO/PO-based polyurethane. Moderate force imaging was used (ratio of the set point amplitude to the free air amplitude was 0.66).

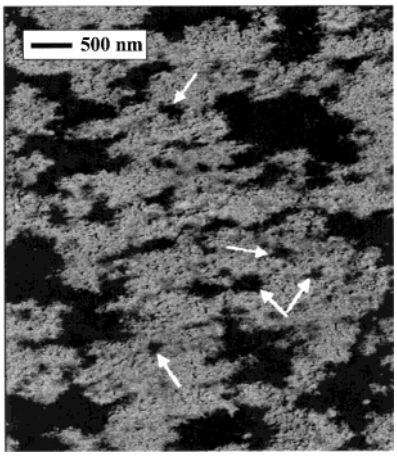


**Figure 10.** Higher magnification ($5 \times 5\ \mu m^2$) phase image of the same sample shown in Figure 9, recorded with same AFM conditions. The arrows indicate some of the larger polyol-rich regions present within the urea aggregates.

A complementary view of the macrophase segregation is seen in the AFM images. Figure 9 presents a relatively low-magnification AFM phase image ($25 \times 25\ \mu m^2$) of the sample. The micron size urea-rich phases induce a greater phase offset and hence appear as the lighter regions in the micrographs. In the same image, polyol-rich regions can be observed which are represented by the darker regions. The force with which a surface is tapped in AFM can be controlled by adjusting the ratio of the set point amplitude to the free air amplitude. In the present study, this ratio was maintained at 0.66, which corresponds to moderate force imaging. No phase inversion was observed on decreasing this ratio to 0.4. Also, there was no observable sample damage due to the sample−tip interaction as rescanning an already scanned area reproduced the original image. A higher magnification ($5 \times 5\ \mu m^2$) phase image of the same sample is presented in Figure 10. This image shows that the urea aggregates are not purely based on urea but also have some polyol residing in them. Some of these polyol regions within the urea aggregates are designated by arrows on the micrograph.

The presence of segregated polyol-rich regions within the precipitates is in agreement with the X-ray microscopy results that show significant polyol within the macrophase precipitates. The presence of polyol in the precipitates and the morphology observed raises the question again as to how the macrophase precipitates form. The understanding of this process continues to evolve. Early explanations of the process suggested that macrophase precipitation begins when a critical molecular weight was reached and discrete spherical precipitates formed.[7] While this suggests a nucleation and growth mechanism, recent results from forced adiabatic in situ studies[11,12,19−21] suggest that spinodal decomposition[49] more adequately explains morphological development in the competition between the thermodynamics of phase segregation and kinetics of polymerization. This recent explanation suggests that thermodynamically driven microphase segregation occurs when the extent of reaction ($N$) and interaction parameter ($\chi$) combined ($\chi N$) force the system across phase boundaries.[20] Hydrogen bonding then occurs in this environment where groups that can hydrogen bond have already come in closer proximity.[50] When the hard segment-rich phase reaches a $T_g$ equal to or greater than the temperature of the foam, hard segment vitrification occurs, resulting in an large increase in the elastic shear modulus ($G'$).

Phase segregation can still occur (the molecular weight at vitrification is still low) with the structure coarsening into more of a droplet structure (Ostwald ripening). It is at this point that the urea macrophase segregation could become prevalent with the resulting morphology being between that expected from spinodal decomposition and nucleation and growth. It should also be noted that poly(urethane−urea)s are a copolymer system with high degree of polydispersity in the sequence lengths.

## 4. Conclusions

X-ray spectromicroscopy of plaques based on high water content slabstock polyurethanes has provided for the first time direct, spatially resolved proof that the macrophase precipitates in these systems are enriched in urea. Analysis of these precipitates in both BO and PO/EO polyol-based plaques validates the chemistry of these phases as urea-rich regions. This information confirms earlier hypotheses based on post-mortem and in situ investigations and provides new insights into the nature of these precipitates.

Macrophase precipitates were found to have 2−4 times the urea content of the matrix, moderate levels of polyol, and low levels of urethane. Analysis of numerous precipitates showed that they were all enriched in urea relative to the adjacent matrix. The contrast in images at 285.2 eV (the aromatic $\pi^*$) was found to roughly equate to the relative urea content. The carbonyl region near 289 eV was critical in correctly identifying the high urea content of the macrophases. Given that urea dominates the precipitates, the 285.2 peak can be used (as in this work) to map urea content in different formulations. Since this sharp, intense peak occurs well below transitions associated with polyol (the main component of polyurethanes by weight), it provides a better handle than the carbonyl signal for studying the spatial distribution of hard segment components. Using this approach, the urea distribution at the boundary/interface between precipitates and matrix was found

to be diffuse, with urea concentration slowly declining over several hundred nanometers from the interface.

There are a large number of competing kinetic and thermodynamic factors that affect polyurethane formation: polymerization to form urethane, polymerization to form urea, phase separation (micro and macro), hydrogen-bonding dynamics, vitrification of the urea hard segment-rich phase, chemical gelation. Thus, it is hardly surprising that characterization of the prevailing multiphase, multi-length-scale morphologies continues to be a significant challenge and learning process. This is one of the driving forces for the development of new and improved techniques with chemical sensitivity at several length scales.

**Acknowledgment.** We thank M. Adams, D. Gier, R. Herrington, and R. Plepys (Dow Chemical) for useful discussions and assistance with this work and G. Young (Dow Chemical) for expert preparation of the polymer thin sections. We also thank M. Elwell for critical review of this manuscript. Data were recorded using the Stony Brook STXM at NSLS X-1A and the BL7.0 STXM at ALS. Financial support has been provided by research and partnership grants from NSERC (Canada) and the Canada Research Chair program. The Stony Brook STXM was developed by the groups of J. Kirz and C. Jacobsen, with support from the Office of Biological and Environmental Research, U.S. DOE under Contract DE-FG02-89ER60858 and the NSF under Grant DBI-9605045. The zone plates were developed by S. Spector and C. Jacobsen of Stony Brook and Don Tennant of Lucent Technologies Bell Labs, with support from the NSF under Grant ECS-9510499. The ALS STXM was developed by T. Warwick (ALS), B. Tonner (UWM), and collaborators, with support from the U.S. DOE (Contract DE-AC03-76SF00098). Zone plates at ALS were provided by Eric Anderson of CXRO, LBNL. H. Ade, G. Appel, and A. P. Smith were supported by NSF Young Investigator Award (DMR-9458060), NSF Grant DMR-0071743, and a grant from Dow Chemical.

## References and Notes

(1) Cooper, S.; Tobolsky, A. *J. Appl. Polym. Sci.* **1966**, *10*, 1837−1844.
(2) Moreland, J. C.; Wilkes, G. L.; Turner, R. B.; Rightor, E. G. *J. Appl. Polym. Sci.* **1994**, *52*, 1459−1468.
(3) Herrington, R. *Flexible Polyurethane Foams*, 2nd ed.; The Dow Chemical Company: 1997. Ulrich, H. Urethane Polymers. *Kirk-Othmer Encyclopedia of Chemical Technology*, 3rd ed; J. Wiley: New York, 1983; Vol. 23, pp 576−608.
(4) Rossmy, G.; Kollmeier, H.; Lidy, W.; Schator, H.; Wiemann, M. *J. Cell. Plast.* **1977**, *13*, 26−35; **1981**, *17*, 319−327.
(5) Brunette, C.; Hsu, S.; MacKnight, W. *Macromolecules* **1982**, *15*, 71−77.
(6) Christenson, C.; Harthcock, M.; Meadows, M.; Spell, H.; Howard, W.; Creswick, M.; Guerra, R.; Turner, R. *J. Polym. Sci., Part B: Polym Phys.* **1986**, *24*, 1401−1439.
(7) Armisted, J.; Wilkes, G.; Turner, R. *J. Appl. Polym. Sci.* **1988**, *35*, 601−629.
(8) Priester, R.; McClusky, J.; O'Neill, R.; Turner, R. *Conf. Proceedings, SPI, Polyurethanes Div.*; Orlando, FL, 1990; pp 527−539.
(9) Artavia, L. D.; Maccosko, C. *Conf. Proceedings Society of the Plastics Institute SPI*; Orlando, FL, 1990; pp 554−561.
(10) McClusky, J.; Priester, R.; O'Neill, R.; Wilkomm, W.; Heaney, M.; Capel, M. *J. Cell. Plast.* **1994**, *30*, 338−360.
(11) Elwell, M.; Ryan, A.; Grunbauer, H.; Van Lieshout, H. *Macromolecules* **1996**, *29*, 2960−2968.
(12) Elwell, M.; Mortimer, S.; Ryan, A. *Macromolecules* **1994**, *27*, 5428−5439.
(13) Koberstein, J.; Stein, R. *J. Polym. Sci., Polym. Phys. Ed.* **1983**, *21*, 1439−1472.
(14) Gier, D.; O'Neill, R.; Adams, M.; Priester, R.; Lidy, W. *Conf. Proceedings Society of the Plastics Institute SPI, Polyurethanes Div.*; Dallas, TX, 1998; pp 278−299.
(15) Lidy, W.; Rightor, E.; Phan Thanh, H.; Dadolle, D. *J. Cell. Plast.* **1997**, *33*, 557−576.
(16) Tabor, R.; Henze, K.; Priestor, R.; Turner, R. *Conf. Proceedings Society of the Plastics Institute SPI*; 1992; pp 514−528.
(17) Lowe, A.; Chandley, E.; Leigh, H.; Molinario, L. *J. Cell. Plast.* **1965**, 127−131.
(18) Lidy, W.; Rightor, E.; Heaney, M.; Davis, B.; Latham, L.; Barnes, G. *Conf. Proceedings Polyurethanes World Congress*; 1997; pp 95−117.
(19) Elwell, M.; Ryan, A.; Grunbauer, H.; Van Lieshout, H. *Polymer* **1996**, *37*, 1353−1361.
(20) Wilkinson, A.; Ryan, A. *Polymer Processing and Structure Development*; Kluwer Publishers: Dordrecht, 1998; Chapters 5−7.
(21) Stanford, J.; Ryan, A.; Elwell, M. In *Materials Science Technology: A Comprehensive Treatment*; Cahn, R., Haasen, P., Kramer, E., Ser. Eds.; Meijer, H., Ed.; VCH Publishers: Weinheim, 1997; Vol. 18, pp 464−512.
(22) Artavia, L.; Macosko, C. *J. Cell. Plast.* **1990**, *26*, 490−511.
(23) Jacobsen, C.; Williams, S.; Anderson, E.; Browne, M. T.; Buckley, C. J.; Kern, D.; Kirz, J.; Rivers, M.; Zhang, X. *Opt. Commun.* **1991**, *86*, 351−364.
(24) Ade, H.; Zhang, X.; Cameron, S.; Costello, C.; Kirz, J.; Williams, S. *Science* **1992**, *258*, 972−975.
(25) Kirz, J.; Jacobsen, C.; Howells, M. *Q. Rev. Biophys.* **1995**, *33*, 33−130.
(26) Ade, H. *Exp. Methods Phys. Sci.* **1998**, *32*, 225−261.
(27) Tennant, D.; Spector, S.; Stein, A.; Jacobsen, C. In *X-ray Microscopy: Proceedings of the Sixth International Conference*; Meyer-Ilse, W., Warwick, A., Attwood, D. T., Eds.; American Institute of Physics: Melville, NY, 2000; pp 601−606.
(28) Rightor, E. G.; Hitchcock, A. P.; Ade, H.; Leapman, R. D.; Urquhart, S. G.; Smith, A. P.; Mitchell, G. E.; Fisher, D.; Shin, H. J.; Warwick, T. *J. Phys. Chem. B* **1997**, *101*, 1950−1961.
(29) Urquhart, S. G.; Ade, H.; Smith, A. P.; Hitchcock, A. P.; Rightor, E. G.; Lidy, W. *J. Phys. Chem. B* **1999**, *103*, 4603−4610.
(30) Urquhart, S. G.; Hitchcock, A. P.; Leapman, R. D.; Priester, R. D.; Rightor, E. G. *J. Polym. Sci., Part B: Polym. Phys.* **1995**, *33* 1593−1602; 1603−1620.
(31) Urquhart, S. G.; Hitchcock, A. P.; Smith, A. P.; Ade, H.; Lidy, W.; Rightor, E. G.; Mitchell, G. E. *J. Electron Spectrosc.* **1999**, *100*, 119−135.
(32) Frommer, J. *Angew. Chem., Int. Ed. Engl.* **1992**, *31*, 1298−1321.
(33) McLean, R. S.; Sauer, B. B. *Macromolecules* **1997**, *30*, 8314−8317.
(34) Kaushiva, B. D.; McCartney, S. R.; Rossmy, G. R.; Wilkes, G. L. *Polymer* **2000**, *41*, 285−294.
(35) Aneja, A.; Wilkes, G. L. Submitted to *J. Appl. Polym. Sci.*
(36) Garrett, J.; Siedlecki, C.; Runt, J. *Macromolecules* **2001**, *34*, 7066−7070.
(37) Guettes, B.; Dinsch, S.; Steinchen, K.; Hoeppner, G.; Wagner, K.; Larbig, H.; Lutter, H. U.S. Patent 5925687, to BASF AG, July 20, 1999.
(38) Bhattacharjee, D.; Latham, D.; Nelson, G.; Legion, C. International Patent WO 98/27132, to Dow Chemical, June 25, 1998.
(39) Ade, H.; Smith, A. P.; Zhang, H.; Zhuang, G. R.; Kirz, J.; Rightor, E. G.; Hitchcock, A. P. *J. Electron Spectrosc.* **1997**, *84*, 53−72.
(40) Warwick, T.; Padmore, H.; Ade, H.; Hitchcock, A. P.; Rightor, E. G.; Tonner, B. *J. Electron Spectrosc.* **1997**, *84*, 85−98.
(41) Warwick, T.; Franck, K.; Kortwight, J. B.; Meigs, G.; Moronne, M.; Myneni, S.; Rotenberg, E.; Seal, S.; Steele, W. F.; Ade, H.; Garcia, A.; Cerasari, S.; Denlinger, J.; Hayakawa, S.; Hitchcock, A. P.; Tyliszczak, T.; Rightor, E. G.; Shin, H.-J.; Tonner, B. *Rev. Sci. Instrum.* **1998**, *69*, 2964−2973.
(42) Ma, Y.; Chen, C. T.; Meigs, G.; Randall, K.; Sette, F. *Phys. Rev. A* **1991**, *44*, 1848−1858.
(43) Jacobsen, C.; Wirick, S.; Flynn, G.; Zimba, C. *J. Microsc.* **2000**, *197*, 173−184.
(44) Coffey, T.; Urquhart, S.; Ade, H. *J. Electron Spectrosc. Relat. Phenom.* **2002**, *122*, 65−78.

(45) Press, W. H.; et al. *Numerical Recipes in C: The Art of Scientific Computing*; Cambridge University Press: Cambridge, 1992.
(46) Zhang, X.; Balhorn, R.; Mazrimas, J.; Kirz, J. *J. Struct. Biol.* **1996**, *116*, 335−344.
(47) Ade, H.; Urquhart, S. G. In *Chemical Applications of Synchrotron Radiation*; Sham, T. K., Ed.; World Scientific: in press.
(48) Koprinarov, I. N.; Hitchcock, A. P.; McCrory, C.; Childs, R. F. *J. Phys. Chem. B* **2002**, *106*, 5358.
(49) Creswick, M.; Lee, K.; Turner, R.; Huber, L. *J. Elastom. Plast.* **1989**, *21*, 179−196.
(50) Bras, W.; Derbyshire, G. E.; Bogg, D.; Cooke, J.; Elwell, M. J.; Komanschek, B. U.; Naylor, S.; Ryan, A. J. *Science* **1995**, *267*, 996−999.
(51) Henke, B. L.; Lee, P.; Tanaka, T. J.; Shimabukuro R. L.; Fujikawa, B. K. *At. Data Nucl. Data Tables* **1982**, *27*, 1−132.
(52) Hamley, I. W. *Introduction to Soft Matter, Polymers Colloids, Amphiphiles and Liquid Crystals*; J. Wiley: New York, 2000; pp 85−90.

MA0122627